Nanoengineering Coaxial Carbon Nanotube–Dual-Polymer Heterostructures

Samuel D. Stranks, Chaw-Keong Yong, Jack A. Alexander-Webber, Christian Weisspfennig, Michael B. Johnston, Laura M. Herz, and Robin J. Nicholas*

Department of Physics, Clarendon Laboratory, Parks Road, Oxford, OX1 3PU, U.K.

ABSTRACT

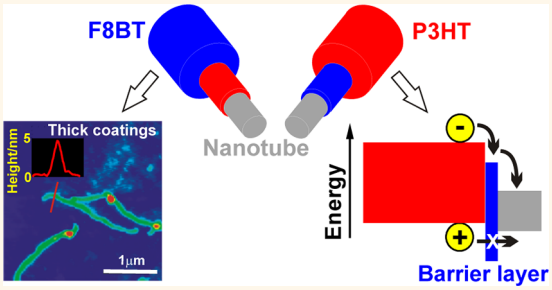

We describe studies of new nanostructured materials consisting of carbon nanotubes wrapped in sequential coatings of two different semiconducting polymers, namely, poly(3-hexylthiophene) (P3HT) and poly(9,9′-dioctylfluorene-*co*-benzothiadiazole) (F8BT). Using absorption spectroscopy and steady-state and ultrafast photoluminescence measurements, we demonstrate the role of the different layer structures in controlling energy levels and charge transfer in both solution and film samples. By varying the simple solution processing steps, we can control the ordering and proportions of the wrapping polymers in the solid state. The resulting novel coaxial structures open up a variety of new applications for nanotube blends and are particularly promising for implementation into organic photovoltaic devices. The carbon nanotube template can also be used to optimize both the electronic properties and morphology of polymer composites in a much more controlled fashion than achieved previously, offering a route to producing a new generation of polymer nanostructures.

KEYWORDS: carbon nanotube · P3HT · F8BT · nanoengineering · molecular heterojunctions · photovoltaic

Single-walled carbon nanotubes (SWNTs) have remarkable electronic and physical properties, with potential applications ranging from optoelectronic devices such as organic photovoltaics (OPVs)[1−3] to high-strength structural composites.[4−6] Combining nanotubes with semiconducting polymers allows the creation of new nanohybrid structures where a layer of polymer is strongly bound to the nanotubes through the $\pi-\pi$ interactions between the conjugated polymer chains and the nanotubes. The polymer layer both prevents nanotube bundling and significantly modifies the electronic and mechanical properties of the nanohybrid structures. An extensive range of polymers have been utilized to date, with the polymers chosen to give enhanced diameter selectivity,[7,8] improved mechanical properties for the blend,[9,10] or controlled electronic modifications. A particularly important example is the formation of a type II heterojunction energy level alignment between small-diameter (<1 nm) SWNTs and porphyrin oligomers[11,12] or poly(3-hexylthiophene) (P3HT),[13,14] allowing excitons in the polymers to dissociate by transferring electrons to the SWNTs.[15] Long-lived charge separation can be achieved when SWNT–P3HT nanohybrids are embedded in an excess matrix of P3HT,[15,16] demonstrating the potential of this system for improving OPV device performance.[17] However, even for the smallest diameter tubes, the barrier for hole transfer from P3HT to the nanotubes is small, leading to a pathway that may reduce the charge separation efficiency. In this work we demonstrate how the introduction of a second polymer layer allows us to further control the electronic properties by molecular engineering the structures to give the potential for enhanced charge separation.

Competitive binding processes are ubiquitous in biological systems. For example many drugs act as enzyme inhibitors by dominating a competitive binding process at the active site for the enzyme.[19,20] Reports of the competitive binding of different species to a nanotube are just beginning to appear. Ju *et al.* have exploited the displacement of chirality-selective flavin mononucleotides by a surfactant to give nanotube chirality enrichment,[21] while Chen *et al.* have observed large differences in the binding of fluorene-based polymers.[22]

* Address correspondence to r.nicholas@physics.ox.ac.uk.

Received for review March 14, 2012 and accepted June 12, 2012.

Published online June 12, 2012
10.1021/nn301133v

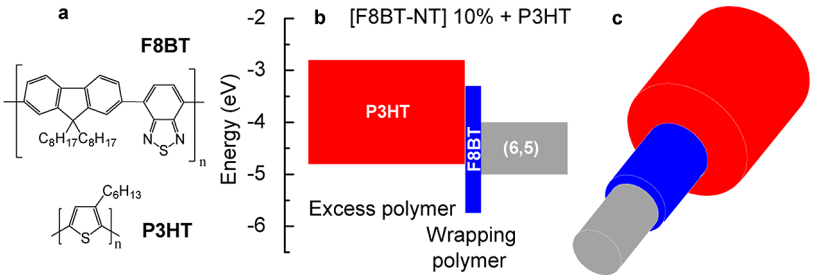

Figure 1. (a) Chemical structures of F8BT (upper) and P3HT (lower). (b) Schematic energy level diagram of nanohybrids consisting of NTs wrapped in F8BT polymer and embedded in an excess P3HT matrix, such that the F8BT constitutes 10% of the total polymer mass. Energies are given with respect to vacuum and are taken from Schuettfort *et al.*[14] and McNeill *et al.*[18] (c) Schematic cartoon to visualize the structure described in (b).

Finally, Sprafke *et al.* showed that there is a strong oligomer length dependence of the binding of porphyrin oligomers to nanotubes, with binding constants differing by orders of magnitudes.[12] However, none of these studies have yet shown any degree of tunability of the final structures.

Here, we show that we can control competitive binding processes to nanoengineer dual-polymer–SWNT structures consisting of nanohybrids of SWNTs coated first with either P3HT or poly(9,9′-dioctylfluorene-*co*-benzothiadiazole) (F8BT) and a second coating of the other polymer as shown schematically in Figure 1c. We show that, despite the intrinsically stronger binding of P3HT to nanotubes when compared to F8BT, we can still selectively manipulate the order of the wrapping to produce a range of different self-assembled structures in the solid state.

The ability to design and construct such nanostructures using simple solution processing techniques opens up a new set of potential applications. For instance, in OPVs a structure with a monolayer of F8BT coating a SWNT embedded in an excess matrix of P3HT (Figure 1b and c) could enhance charge separation by cascading electrons onto the nanotube while blocking recombination of holes with nanotube electrons. Significantly, this could also allow improved charge separation in blends with intermediate to larger diameter tubes (>1 nm), which do not form type II heterojunctions with P3HT.

RESULTS AND DISCUSSION

We investigate the binding competition between polymers by studying the optical properties of nanohybrids prepared first with one polymer and then with the addition of an excess of the second polymer to the solution. The nanohybrids consisting of CoMoCAT SWNTs coated with P3HT or F8BT polymers were synthesized (see Methods) and denoted [P3HT-NT] and [F8BT-NT], respectively. In these pure ("100%") nanohybrids, the only polymer present is attached to the tubes. Increasing amounts of excess polymers were added to the solutions to give a range of concentrations denoted, for example, as [F8BT-NT] *X*% + P3HT, where *X* is the mass percentage of the initial wrapping polymer (F8BT) in the excess polymer (P3HT).

The immediate dielectric environment of the SWNTs directly influences the nanotube band gaps by altering the Coulomb energies of the nanotube excitons.[23] A semiconducting polymer bound to a nanotube screens the Coulomb interactions, giving a net red shift of the optical transition energy relative to a bare nanotube because the electron–electron interactions are larger than the electron–hole components.[23−25] When the energy levels in the polymer form a type II heterojunction, as occurs for P3HT with small-diameter nanotubes, the wave function of the hole on the nanotube is also extended onto the polymer, effectively giving a larger diameter nanotube.[14] This leads to a further red shift of the transition energies compared to other type I blends such as [F8BT-NT]. We use the enhanced red shifts of the E_{11} or E_{22} transitions to probe the immediate environment of the nanotubes and determine which polymer is bound.

Photoluminescence excitation (PLE) maps of the [F8BT-NT] and [P3HT-NT] nanohybrid samples taken in chloroform solution are shown in Figure 2a and b. The nanotube resonances of the distribution are observed, corresponding to excitation of the E_{22} transitions and emission from E_{11}, along with E_{11} emission resulting from energy transfer to the nanotube following absorption in either F8BT[26] (450–550 nm) or P3HT[27] (450–650 nm).

An emission spectrum for the 100% [F8BT-NT] solution is shown at the bottom of Figure 2c for selective excitation at the E_{22} transitions (580 nm) of the (6,5) and (8,4) tubes[28] and for 100% [P3HT-NT] in Figure 2d. The E_{11} transitions for [F8BT-NT] are at 998 and 1133 nm, and for [P3HT-NT] the additional red shift moves them to 1021 and 1141 nm. When an increasing proportion of P3HT is added to the [F8BT-NT] solution (Figure 2c), the spectra show a progressive exchange of intensity from the original peak to one that corresponds to tubes coated with P3HT. Similar behavior is also observed for (7,5) and (7,6) tubes with excitation at 657 nm[28] and for absorption data (see Supporting Information). These observations provide direct evidence for substitution of the F8BT chains on the nanotubes by the excess P3HT chains.

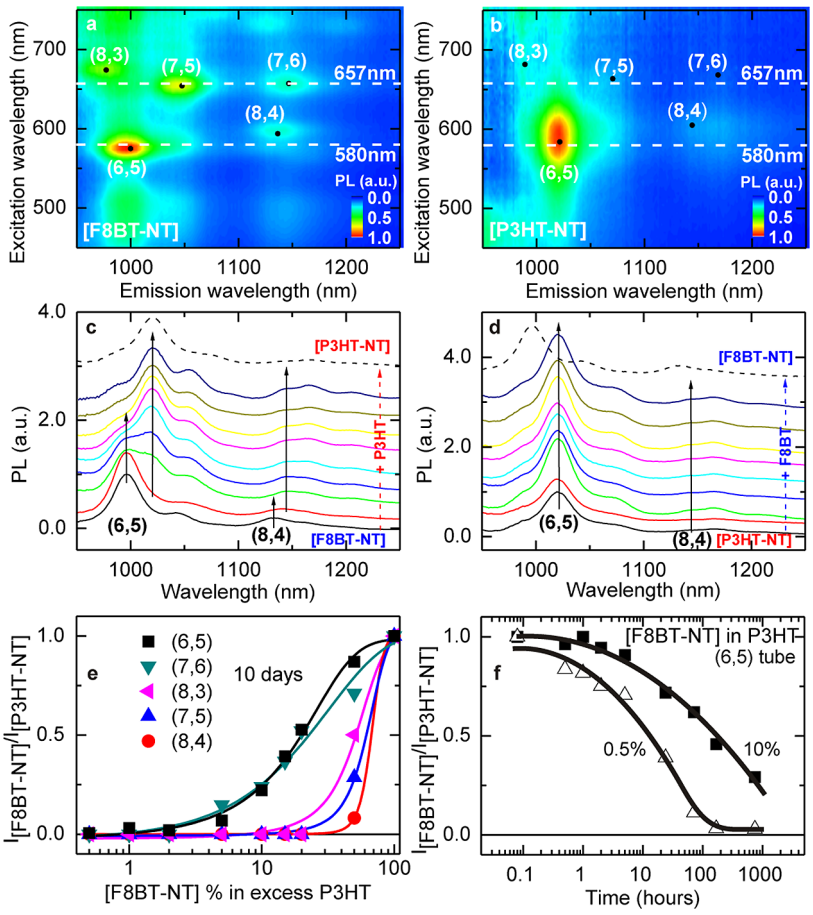

Figure 2. PLE maps of (a) [F8BT-NT] and (b) [P3HT-NT] nanohybrids in chloroform solution with resonant nanotube peaks labeled. The concentration of the wrapping polymer in solution is fixed to an absolute value of 0.006 mg/mL. (c and d) Spectra corresponding to the solutions in (a) and (b) excited at 580 nm with an increasing amount of excess (c) P3HT and (d) F8BT, respectively, and measured 10 days after addition of excess polymer. The nanohybrid proportion progresses through 100, 50, 20, 15, 10, 5, 2, 1, and 0.5% from bottom to top, and spectra are offset for clarity with any excess polymer emission tail subtracted. For reference, emission from the [P3HT-NT] and [F8BT-NT] nanohybrids is also shown (dotted lines). (e) Relative proportion of F8BT−nanotube peaks to P3HT−nanotube peaks with increasing excess P3HT from right to left, as fitted from spectra excited at 580 and 657 nm. Solid lines are guides to the eye. (f) As in (e) but following the time evolution of the (6,5) tubes over a time period of 1 month for 10% and 0.5% [F8BT-NT] proportions in excess P3HT. To obtain these data, fits were carried out on absorption spectra (see Supporting Information). Solid lines are guides to the eye.

The proportions of each nanotube environment (F8BT or P3HT) were deduced by fitting the intensity of the peaks and are plotted in Figure 2e for five nanotube chiralities. The substitution process depends on the type of tube, with a larger excess of P3HT required to displace F8BT from (6,5) and (7,6) tubes. The process also has a considerable time dependence with changes occurring within minutes to days and even weeks (Figure 2f). The process is faster when the proportion of excess polymer is higher, and we also expect faster substitution for larger absolute concentrations, as in the solutions used to cast thin films. By contrast, no substitution is observed for the addition of F8BT to [P3HT-NT] (Figure 2d) on any time scale (see Supporting Information). This indicates that the binding to nanotubes by P3HT is much stronger than by F8BT.

We study the final equilibrium state of the dual polymer structures by isolating the substituted polymer-wrapped nanotubes following immersion in a large excess of the second polymer, which is then removed after 3 days using a solvent extraction process (see Methods), as shown schematically as schemes A and B in Figure 3a. Absorption spectra for spun-cast films are shown in Figure 3b. The product of Scheme A, [F8BT-NT] in P3HT, shows no evidence of the F8BT absorption at 450 nm and therefore only contains P3HT and nanotubes. The P3HT entirely displaces the bound F8BT, which is removed in the extraction process. Conversely, Scheme B, [P3HT-NT] in F8BT, contains both F8BT and P3HT in an approximately 1:1 ratio. While F8BT does not induce displacement of P3HT from the nanotubes, F8BT binds strongly to the [P3HT-NT] system and is not removed even with vigorous solvent extraction.

An atomic force microscopy (AFM) image of the product of Scheme A is shown in Figure 3c and reveals typical heights of ~2 nm. This is consistent with the

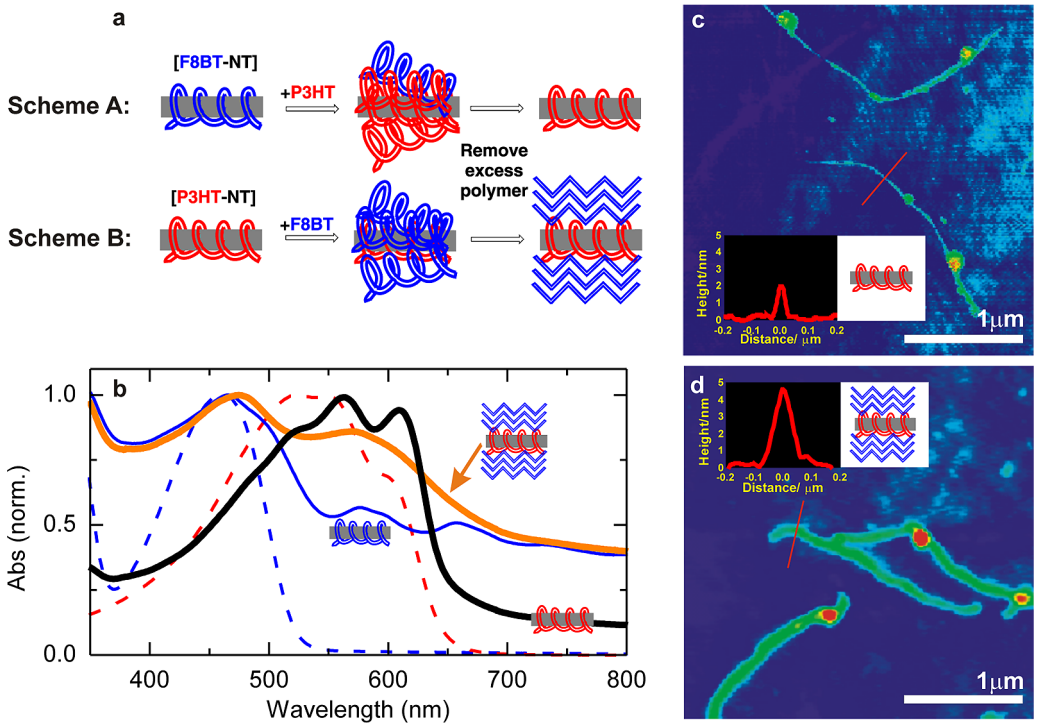

Figure 3. Isolation of nanohybrid species following substitution. (a) Scheme A shows excess P3HT being added to [F8BT-NT] nanohybrids, such that there is a 1% concentration of wrapped polymer out of total polymer. Three days after the addition of excess polymer, any unbound polymer is removed (polymers inverted in Scheme B). The products are discussed in the text. (b) Absorption spectra of the final products taken from spin-coated films are shown with the black line (Scheme A) and orange line (Scheme B). [F8BT-NT] nanohybrid (blue line), F8BT (dashed blue line), and P3HT (dashed red line) spectra are presented for reference, and all spectra are normalized at the polymer peaks. False-color AFM images of the products from (c) Scheme A and (d) Scheme B. The insets show the height analyses across the sections indicated.

binding of only one or two layers of P3HT to a typical CoMoCAT nanotube (height 0.7−0.9 nm) separated by twice the van der Waals radius of carbon (0.34 nm).[27] In addition, some large, isolated P3HT nanocrystals are observed.[27] Very similar images and height analyses are found when an analogous process of adding excess P3HT to [P3HT-NT] nanohybrids and removing any excess polymer is performed (see Supporting Information). This suggests that the nanohybrids bind only a single P3HT layer and any further binding is inhibited by the structure that is formed.

By contrast, the image of the product of Scheme B in Figure 3d shows much thicker uniform polymer coatings ~5 nm in height. The absorption measurements indicate that the two polymers are present in a 1:1 ratio but that some polymer is contained in isolated nanocrystals, probably formed from P3HT.[27] The absorption and emission spectroscopy show that the tubes are still coated entirely by a first layer of P3HT. We conclude that there is a strong binding between the excess F8BT and the initial P3HT wrapping layer. Once F8BT is bound to the structure, this seeds further deposition of F8BT chains, resulting in thick outer layers of F8BT.

The solution studies have shown that excess P3HT added to [F8BT-NT] nanohybrids will eventually displace the F8BT from the tube surface. However a significant amount of the displacement occurs over several hours, meaning that it is possible to retain the F8BT inner layer and create a nanohybrid heterostructure provided that the [F8BT-NT] + P3HT films are prepared quickly in order to "fix" the desired polymer configurations. Conversely, [P3HT-NT] + F8BT nanohybrids can be created without any time constraint.

To investigate the formation of "fixed" nanohybrids in the solid state, thin uniform films were prepared by spin-coating from [P3HT-NT] and [F8BT-NT] nanohybrid solutions with a range of concentrations of either excess F8BT or P3HT. The films were initially cast within 2 h of adding the excess polymers to the nanohybrids, and the final polymer proportions were determined from absorption spectroscopy. The positions of the (6,5) E_{11} absorption peaks are plotted in Figure 4a.

For both [F8BT-NT] and [P3HT-NT] nanohybrids, a small red shift is observed as an increasing excess of the same polymer is added due to the increased thickness of dielectric material around the tubes, which further decreases the Coulomb interactions and red-shifts the transitions.[14] This effect is particularly large when F8BT is added to the [P3HT-NT] nanohybrids, supporting the conclusions of the previous section that thick layers of F8BT bind strongly to the [P3HT-NT] nanohybrids.

When the [F8BT-NT] nanohybrid concentration falls below ~10% in P3HT, the transitions begin to red-shift

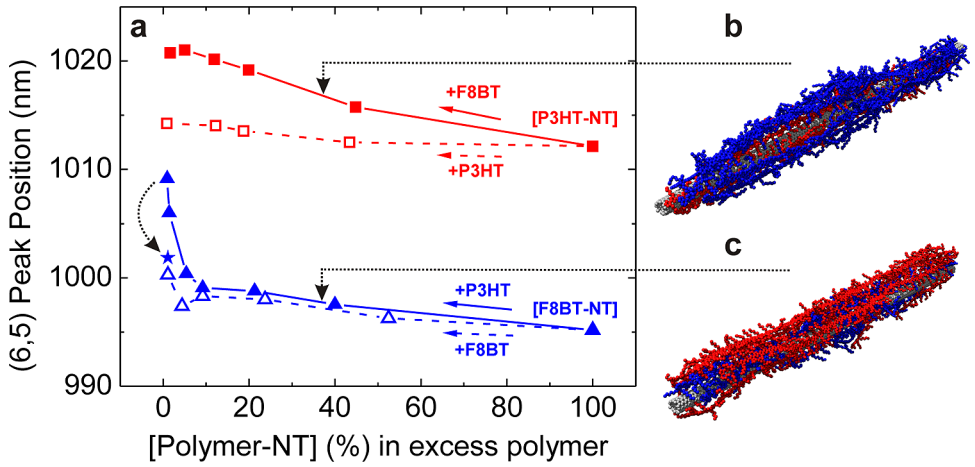

Figure 4. (a) Position of the (6,5) nanotube peak as fitted from absorption spectra of these films (see Supporting Information) spun-cast within 2 h of adding various excess polymer to [P3HT-NT] or [F8BT-NT] solutions. The blue triangle series shows [F8BT-NT] nanohybrids with increasing F8BT (open symbols) and P3HT (closed symbols) from right to left, while the red square series shows [P3HT-NT] nanohybrids with increasing P3HT (open symbols) and F8BT (closed symbols). The blue starred symbol represents a [F8BT-NT] 1% + P3HT sample prepared quickly. Snapshots taken from molecular dynamics simulations to represent the (b) [F8BT-NT] + P3HT and (c) [P3HT-NT] + F8BT nanohybrids, respectively, with the indicated nanohybrid proportions in excess polymer. P3HT chains are in red, F8BT chains in blue, and (6,5) nanotubes in gray.

rapidly and approach the P3HT-like (6,5) values. This confirms that the bound F8BT is displaced by P3HT when in large excess. All film properties are stable with time, and the preparation time window of 2 h is sufficient to "fix" the structure for samples with a nanohybrid concentration of greater than ~10%. This can be extended to films with a larger excess of polymer by casting films on an even faster time scale, as can be seen by the peak position of a [F8BT-NT] 1% + P3HT sample prepared in ~10 min (starred symbol), which shows much less red shift.

Further evidence for the structure of the nanohybrids comes from studying the photoluminescence (PL) from the polymers (Figure 5a). As the proportion of [F8BT-NT] nanohybrids in the excess P3HT matrix increases from 1% to 50%, the P3HT component (600−850 nm) blue-shifts with a corresponding increase in the intensity of the highest energy (0−0) peak. This is attributed to a disruption of the P3HT aggregation[29] by the addition of nanohybrids, as observed previously.[15]

Figure 5b shows that as increasing amounts of F8BT are added to the [P3HT-NT] nanohybrids, the P3HT emission shows a significantly larger blue shift with an even greater increase in the 0−0 peak. This is attributed to a phase separation on a single-chain level. The blue shift is enhanced because the P3HT chains have been further isolated by the thick F8BT coatings, as observed in the AFM images (Figure 3d). Significant F8BT emission is observed only when there is very little or no P3HT present.

In order to understand the differences in substitution dynamics for the nanostructures and visualize the final structures, molecular dynamics simulations were carried out. These use F8BT chains consisting of 13 repeat units (~1/3 of the length of actual F8BT chains) matched in length to P3HT chains (40 thiophene repeating units; ~1/7 of the length of actual P3HT chains). The binding of six chains of one polymer type to a (6,5) nanotube of length 30 nm was simulated, and the results were similar to those observed previously.[30]

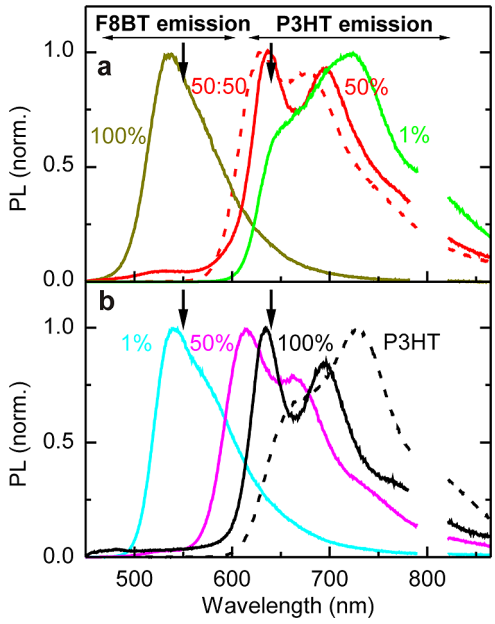

Figure 5. Steady-state PL polymer spectra from film samples of (a) [F8BT-NT] 1% (green) and 50% (red) in excess P3HT, [F8BT-NT] 100% (dark yellow), and a 50:50 F8BT:P3HT blend (red dashed) and (b) [P3HT-NT] 1% (cyan) and 50% (magenta) in excess F8BT, [P3HT-NT] 100% (black), and P3HT (black dashed). Samples were excited at 400 nm, and spectra are normalized to the peak emission. The laser fundamental at 800 nm has been removed from the spectra. Arrows denote detection wavelengths for PLUC measurements (550 and 640 nm).

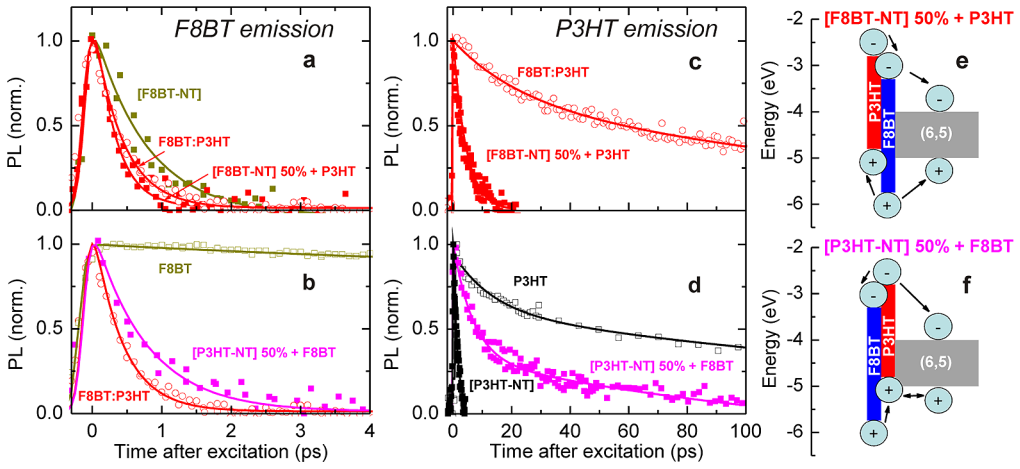

Figure 6. Time-resolved PLUC measurements following photoexcitation at 400 nm to monitor the F8BT emission at (a, b) 550 nm and P3HT emission at (c, d) 640 nm from film samples of [F8BT-NT] 50% + P3HT (red closed squares), 50:50 F8BT:P3HT (red open circles), [F8BT-NT] (dark yellow closed squares), F8BT (dark yellow open squares), [P3HT-NT] 50% + F8BT (magenta closed squares), [P3HT-NT] 100% (black closed squares), and P3HT (black open squares). Solid lines represent mono- and multiexponential fits to the data, convoluted with the Gaussian system response function (220 fs). Schematics to show the energy level alignments of the species in the (e) [F8BT-NT] 50% + P3HT and (f) [P3HT-NT] 50% + F8BT nanohybrids and the electronic processes occurring between the materials. The double-headed arrow in (f) represents the delocalization of holes across both P3HT and the nanotube because of the small barrier for P3HT-to-tube hole transfer.

After the systems reached equilibrium, 10 chains of the other polymer were added and the simulations continued (see Supporting Information for additional simulations).

The resulting [F8BT-NT] + P3HT structure is shown in Figure 4b. In this model and in other simulations, P3HT does not bind favorably to F8BT but preferentially binds to any exposed areas of nanotubes. The P3HT monomers are less rigid than those of F8BT, allowing the greater flexibility of the polymer to explore any exposed nanotube surfaces. This could explain the mechanism for the substitution process.

By contrast, the simulations of the [P3HT-NT] system with added F8BT polymer (Figure 4c) show that the F8BT chains favorably adsorb to the already bound P3HT chains. This results in a uniform outside coating of relatively flat F8BT chains onto which additional F8BT chains can bind.

To investigate the electronic dynamics in the nanohybrid structures formed, we study time-dependent photoluminescence of the wrapping and excess polymers in the prepared films, using PL upconversion with 220 fs time resolution. Measurements were taken with excitation at 400 nm and detection at 640 and 550 nm, corresponding to P3HT and F8BT emission, respectively. We concentrate our discussion on the 50% blend samples, for which excitons are created in the F8BT and P3HT components in a ratio of ~2:1 according to absorption spectra, and no excitons are initially created in the semiconducting nanotubes.

Figure 6a and b show that emission from F8BT (550 nm) is quenched remarkably quickly in the presence of either nanotubes or P3HT. Films of F8BT alone have a relatively long emission lifetime of over 1000 ps, while all blends investigated show rapid quenching with lifetimes below 0.8 ps. The reasons for these fast dynamics lie in both the electronic structure and morphology of the nanoscale interfaces. Energy level schematics shown in Figure 6e and f illustrate that F8BT excitons may be quenched through both energy and charge transfer at interfaces with either P3HT or (6,5) nanotubes, thus opening a multitude of decay pathways. As illustrated by the molecular modeling simulations, the favorable binding of F8BT to P3HT also aids the overall fast excitation transfer into P3HT. The short F8BT emission lifetime of 0.42 ps measured for all-polymer 50:50 P3HT:F8BT blend films (Figure 6a) suggests that intimate mixing of these two polymers alone is sufficient to induce rapid exciton quenching in the F8BT phase. In addition, the order of arrangement in the coaxial nanotube polymer structures clearly influences the excitation transfer dynamics. For dual-polymer-wrapped nanotubes containing F8BT on the outside ([P3HT-NT] 50% + F8BT, Figure 6b) the quenching of F8BT emission is slower (0.77 ps lifetime) than for the case for which F8BT is sandwiched between P3HT and the nanotubes ([F8BT-NT] 50% + P3HT, Figure 6a, 0.29 ps lifetime).

Figure 6c shows that the time dependence of P3HT emission at 640 nm is appreciably slower than observed for F8BT emission for all samples investigated. The reasons for such slowed dynamics can be mostly attributed to the absence of efficient excitation transfer from P3HT to F8BT. The P3HT emission from the P3HT:F8BT 50:50 blend is dominated by a long-lived 220 ps component also observed in the lower resolution time-correlated single photon counting results (see Supporting Information). By contrast, the presence of carbon nanotubes, around which both P3HT and

F8BT wrap, introduces rapid decay mechanisms for P3HT excitations. Figure 6c shows that the P3HT emission for the [F8BT-NT] 50% + P3HT sample has an initial decay time constant of 4.4 ps and is quenched almost completely to zero within 20 ps after excitation. These decay dynamics are significantly slower than those observed for pure [P3HT-NT] nanohybrids (Figure 6d), for which we observe picosecond P3HT emission decay. The introduction of an F8BT layer between P3HT and the nanotubes thus leads to a measurable inhibition of excitation transfer between the two and in the reverse process may block recombination once charge separation has been established. Figure 6e illustrates these processes: excitons created on the P3HT can be dissociated at the interface with F8BT, with electrons cascading to the F8BT and then to the nanotube, while holes may remain within the P3HT.

By contrast, reversing the ordering of the wrapping, *i.e.*, [P3HT-NT] 50% + F8BT, leads to a two-component longer lived decay of the P3HT emission (Figure 6d). The initial fast component decays with a time constant of 6.8 ps, followed by a slower component with time constant of ~150 ps. The appearance of a much longer lived component demonstrates the influence of the very different electronic structure for the [P3HT-NT] + F8BT nanohybrids, as illustrated in Figure 6f. The addition of F8BT to [P3HT-NT] provides an alternative pathway for excitons on P3HT chains to dissociate by transferring electrons into the F8BT cladding layer. A significant number of the electrons transferred to the F8BT are likely to eventually tunnel back into the P3HT in the varied energy landscape that will be created by the polymer wrapping process (Figure 4c), thus enabling them to recombine with the longer lived excess holes in the [P3HT-NT], giving rise to the longer lived component of the P3HT emission.

The energy levels shown in Figure 6e and f suggest that both [F8BT-NT] + P3HT and [P3HT-NT] + F8BT structures can offer important advantages for nanotechnology applications. When the initial layer is F8BT, it may act as a barrier layer, preventing holes created in the P3HT from recombining with electrons in the nanotubes, even for larger diameter tubes. The structure provides a means to physically separate electrons and holes onto different materials separated by an energetic barrier, through bottom-up self-assembly. By incorporating an excess of P3HT to allow the hole to move away from the interface,[15] these structures could be integrated into OPVs, enabling the nanotubes to be used as electron transporters.[17] When P3HT is the initial wrapper, the [P3HT-NT] nanohybrids act as a template to bind thick layers of F8BT polymer. Such preferential binding effects may prove useful in providing nanotube-seeded blend morphologies optimized for OPV that are difficult to achieve in polymer−polymer blends.[31−34]

CONCLUSIONS

In conclusion, we have engineered new nanostructures consisting of single-walled carbon nanotubes coated with sequential layers of the semiconducting polymers P3HT and F8BT. Solution spectroscopy measurements reveal that P3HT has a much stronger binding affinity to the nanotubes and, in the presence of a large excess, slowly displaces F8BT from the tube surface. However, by varying the order and timing of the processes, the ordering and proportions of the wrapping polymers can be controlled to give a wide range of final structures. The coating process is naturally self-limiting, and layers of the materials can be deposited as thin films for use in device applications. The use of ultrafast photoluminescence spectroscopy shows that the new band alignments of these nanostructures dramatically change their electronic properties, suggesting their potential for controlling phenomena such as electron and hole transfer between materials. By exploiting the favorable energy alignments combined with the high mobilities of the nanotubes, these novel nanostructures may be useful for a variety of devices such as organic photovoltaics.

At a more general level, the use of the carbon nanotube template has allowed us to produce a completely new type of nanostructure in which the polymer layers can be deliberately engineered to give a specifically ordered structure, and we can speculate that this may even lead to the production of new multiple layered structures in which the electronic properties can be tuned in an analogous way to semiconductor superlattices and quantum wells. The carbon nanotube template also offers the possibility of structural engineering of the polymer blends, thus enabling better control of the morphology of polymer composites and offering a route to a new generation of polymer nanostructures.

METHODS

Preparation of Nanohybrid Solutions. Regioregular poly(3-hexylthiophene-2,5-diyl) (P3HT) with average molecular weight 50 000 g mol^{-1} and poly[9,9-dioctylfluorenyl-2,7-diyl)-co-1,4-benzo-2,1′-3-thiadiazole)] (F8BT) with molecular weight 30 000 g mol^{-1} were used as received from Rieke Metals, Inc. and American Dye Source, Inc., respectively. CoMoCAT nanotubes with small-diameter (0.7−0.9 nm) and >90% semiconducting tube purity were purchased from SouthWest Nanotechnologies. All solvents were purchased from Sigma-Aldrich.

The [P3HT-NT] nanohybrids were synthesized as described elsewhere.[15,27] In the synthesis process, P3HT was dissolved in chlorobenzene solution to a 0.6 mg/mL concentration, and CoMoCAT material was added to 0.3 mg/mL. The dispersion was

treated in an ultrasonic disintegrator for 15 min, followed by centrifugation for 8 min at 10000*g*. The excess P3HT polymer was removed by adding toluene to a 2:1 volume ratio, inducing aggregation of the nanostructures and precipitation after centrifugation for 4 min at 16000*g*. The supernatant containing the excess P3HT was discarded, and the residue redissolved in fresh toluene. This purification process was repeated a further two times. Finally, the highly purified nanostructure residue was redissolved in chloroform to a high concentration. The [F8BT-NT] nanohybrids were synthesized in the same manner, except using polymer and CoMoCAT starting concentrations of 0.5 mg/mL.

To determine the mass concentration of wrapping polymer, absorption spectra (Perkin-Elmer Lambda 9 UV−vis−NIR spectrophotometer) of the diluted nanohybrid solutions were compared to spectra of pure polymers at a known concentration. Typical wrapped polymer concentrations were 0.6 mg/mL for [P3HT-NT] and 0.4 mg/mL for [F8BT-NT].

Solution Binding Competition Absorption and PL. A series of dilute chloroform solutions (diluted to 1/100) of [F8BT-NT] and [P3HT-NT] nanohybrids were prepared and briefly tip sonicated to prevent aggregation. Excess polymers (series of F8BT and P3HT for both nanohybrids) were added to give the percentages of wrapping polymer in excess polymer quoted in the text. All solutions were stored in the dark to prevent sample photodegradation. Photoluminescence excitation maps were acquired on a custom-built setup[7] consisting of a 75 W xenon lamp focused into a monochromator, which then illuminated the mounted film or solution cuvette samples. The PL was collected at 90° to the excitation beam and focused into a spectrograph fitted with a liquid nitrogen-cooled InGaAs photodiode array. The excitation beam intensity was normalized using a silicon photodiode, and the spectra were corrected for instrumental response using a tungsten filament lamp of known emissivity.

Isolating Substituted Nanohybrids. Solutions of each nanohybrid were tip sonicated, and each combination of excess polymer was added to achieve nanohybrid concentrations of 1%. The solutions were left for 3 days after polymer addition, and, after this time, the [F8BT-NT] 1% + P3HT sample was observed to be completely substituted using absorption and PL spectra. To remove the excess polymer, twice the volume of toluene was added to induce aggregation and the solutions were centrifuged for 4 min at 16000*g*. The supernatant containing the unwrapped excess polymer was discarded, the pellet residue redissolved in fresh toluene, and the process repeated at least five times. The final residue was redissolved in a concentrated chloroform solution, and a portion used to spin-coat a film on plasma-etched quartz substrates (120 s, 200 rpm), followed by an annealing treatment at 120 °C for 30 min.

AFM images were obtained using a ThermoMicroscope M5 in noncontact mode. Samples were prepared by spin-coating a diluted (1/100) solution at 2000 rpm on a flat quartz substrate, followed by annealing at 180 °C for 15 min.

Preparation of Nanohybrid Films. Thin, uniform films were prepared by spin-coating the concentrated chloroform solutions of [P3HT-NT] and [F8BT-NT] nanohybrids onto plasma-etched quartz substrates at 200 rpm for 120 s. In order to make 50% blends, an equal mass concentration of the desired excess polymer was added from a concentrated stock solution, and films were spun in a similar manner. Since the polymers aggregate significantly when spun-cast slowly at high concentrations, higher spin speeds (1000 rpm, 60 s) were required to achieve uniform films for the nanohybrid concentrations of 20% and below. In addition, the differing densities and solubilities of the polymer and nanohybrid species meant that the final ratios did not scale linearly with starting concentration. As such, the total mass concentration was varied between 5 and 10 mg/mL and the films were checked to have the correct ratios using absorption spectroscopy (see Supporting Information for details). Polymer controls containing no NTs were also spin-coated at 1000 rpm (60 s) from solutions with a total polymer concentration fixed at 10 mg/mL. To prevent degradation, all film preparation and storage was conducted in a nitrogen glovebox with an oxygen concentration of <1.5 ppm. All films were cast quickly (<2 h after polymer addition, <10 min for the [F8BT-NT] 1% + P3HT sample for polymer PL measurements), without allowing sufficient time for significant substitution to occur, and annealed at 120 °C for 30 min.

Molecular Dynamics Simulations. Molecular structures were constructed using HyperChem (Hypercube Inc.) software with the (6,5) carbon nanotube coordinates (length 30 nm) generated using Nanotube Modeler. P3HT (40 units) and F8BT polymer (13 units) chains were built to be of equal length and relaxed with the conjugate gradient method. Simulations were carried out using the Tinker package[35] with the MM3 force field[36] and a simulation box of size 2000 × 2000 × 2000 Å^3. Molecular dynamics time steps of 1.0 fs were taken by means of a modified Beeman algorithm,[37] and a Bussi−Parrinello thermostat[38] was used for temperature control (298 K). Carbon nanotube atoms were fixed to reduce computation time, as has been implemented elsewhere,[30,39] and this was not seen to affect the adsorption dynamics or energies. The starting configurations of the polymers did not significantly affect the final results. Ray-traced images of the results were created using POV-Ray in the UCSF Chimera package.[40]

Polymer Photoluminescence Measurements. Film samples were excited at 400 nm using the output of a mode-locked Ti:sapphire laser (Spectra-Physics Tsunami), with pulses of duration 100 fs and at a repetition rate of 80 MHz, frequency-doubled using a barium borate (BBO) crystal. The incident fluence was adjusted using a half-wave plate and polarizer. A Si CCD detector was used to acquire the steady-state PL emission, and all spectra were corrected for instrumental response using a tungsten filament lamp of known emissivity. Film measurements were carried out under vacuum (<10^{-4} mbar) to prevent film degradation.

In the photoluminescence upconversion (PLUC) technique[41] (220 fs resolution), the emerging PL was collected using a pair of off-axis parabolic mirrors and focused onto a BBO crystal mounted on a rotation stage to allow tuning of the phase-matching angle. A gate beam (800 nm) arriving at the BBO crystal at adjustable time delays was used to up-convert the PL at given times after excitation. The resulting sum-frequency photons were collected, dispersed in a monochromator, and detected by a liquid nitrogen-cooled CCD detector. For time-correlated single photon counting (TCSPC) measurements (120 ps system resolution), the CCD detector was replaced by a photomultiplier tube, and a fraction of the 800 nm Ti:Sapphire output was directed onto a Si-PIN diode, providing the trigger pulse for a signal period for the measurements. Fluences of 150 and 9 nJ/cm^2 were used for PLUC and TCSPC, respectively.

PLUC data were fitted using mono- or biexponential functions convoluted with the Gaussian system response function (220 fs). For the biexponential fits, the time constants corresponding to the slow components were fixed to the values obtained from monoexponential fits to the TCSPC data (see Supporting Information).

Conflict of Interest: The authors declare no competing financial interest.

Acknowledgment. The authors thank the Engineering and Physical Sciences Research Council for their financial support and H. J. Snaith for useful discussion. S.D.S. acknowledges the Rhodes Trust for financial support.

Supporting Information Available: Additional PL and absorption spectra, AFM images, molecular dynamics simulations, and TCSPC results. This material is available free of charge *via* the Internet at http://pubs.acs.org.

REFERENCES AND NOTES

1. Kymakis, E.; Servati, P.; Tzanetakis, P.; Koudoumas, E.; Kornilios, N.; Rompogiannakis, I.; Franghiadakis, Y.; Amaratunga, G. A. J. Effective Mobility and Photocurrent in Carbon Nanotube-Polymer Composite Photovoltaic Cells. *Nanotechnology* **2007**, *18*, 435702.
2. Ham, M. H.; Paulus, G. L. C.; Lee, C. Y.; Song, C.; Kalantar-Zadeh, K.; Choi, W.; Han, J. H.; Strano, M. S. Evidence for High-Efficiency Exciton Dissociation at Polymer/Single-Walled

Carbon Nanotube Interfaces in Planar Nano-Heterojunction Photovoltaics. *ACS Nano* **2010**, *4*, 6251–6259.
3. Bindl, D. J.; Wu, M. Y.; Prehn, F. C.; Arnold, M. S. Efficiently Harvesting Excitons from Electronic Type-Controlled Semiconducting Carbon Nanotube Films. *Nano Lett.* **2011**, *11*, 455–460.
4. Ajayan, P. M.; Schadler, L. S.; Giannaris, C.; Rubio, A. Single-Walled Carbon Nanotube-Polymer Composites: Strength and Weakness. *Adv. Mater.* **2000**, *12*, 750–753.
5. Moniruzzaman, M.; Winey, K. I. Polymer Nanocomposites Containing Carbon Nanotubes. *Macromolecules* **2006**, *39*, 5194–5205.
6. Koziol, K.; Vilatela, J.; Moisala, A.; Motta, M.; Cunniff, P.; Sennett, M.; Windle, A. High-Performance Carbon Nanotube Fiber. *Science* **2007**, *318*, 1892–1895.
7. Nish, A.; Hwang, J. Y.; Doig, J.; Nicholas, R. J. Highly Selective Dispersion of Single-Walled Carbon Nanotubes Using Aromatic Polymers. *Nat. Nanotechnol.* **2007**, *2*, 640–646.
8. Ozawa, H.; Fujigaya, T.; Niidome, Y.; Hotta, N.; Fujiki, M.; Nakashima, N. Rational Concept to Recognize/Extract Single-Walled Carbon Nanotubes with a Specific Chirality. *J. Am. Chem. Soc.* **2011**, *133*, 2651–2657.
9. Coleman, J. N.; Cadek, M.; Ryan, K. P.; Fonseca, A.; Nagy, J. B.; Blau, W. J.; Ferreira, M. S. Reinforcement of Polymers with Carbon Nanotubes. The Role of an Ordered Polymer Interfacial Region. Experiment and Modeling. *Polymer* **2006**, *47*, 8556–8561.
10. Carey, B. J.; Patra, P. K.; Ci, L.; Silva, G. G.; Ajayan, P. M. Observation of Dynamic Strain Hardening in Polymer Nanocomposites. *ACS Nano* **2011**, *5*, 2715–2722.
11. Stranks, S. D.; Sprafke, J. K.; Anderson, H. L.; Nicholas, R. J. Electronic and Mechanical Modification of Single-Walled Carbon Nanotubes by Binding to Porphyrin Oligomers. *ACS Nano* **2011**, *5*, 2307–2315.
12. Sprafke, J. K.; Stranks, S. D.; Warner, J. H.; Nicholas, R. J.; Anderson, H. L. Noncovalent Binding of Carbon Nanotubes by Porphyrin Oligomers. *Angew. Chem., Int. Ed.* **2011**, *50*, 2313–2316.
13. Kanai, Y.; Grossman, J. C. Role of Semiconducting and Metallic Tubes in P3HT/Carbon-Nanotube Photovoltaic Heterojunctions: Density Functional Theory Calculations. *Nano Lett.* **2008**, *8*, 908–912.
14. Schuettfort, T.; Nish, A.; Nicholas, R. J. Observation of a Type II Heterojunction in a Highly Ordered Polymer-Carbon Nanotube Nanohybrid Structure. *Nano Lett.* **2009**, *9*, 3871–3876.
15. Stranks, S. D.; Weisspfennig, C.; Parkinson, P.; Johnston, M. B.; Herz, L. M.; Nicholas, R. J. Ultrafast Charge Separation at a Polymer-Single-Walled Carbon Nanotube Molecular Junction. *Nano Lett.* **2011**, *11*, 66–72.
16. Ferguson, A. J.; Blackburn, J. L.; Holt, J. M.; Kopidakis, N.; Tenent, R. C.; Barnes, T. M.; Heben, M. J.; Rumbles, G. Photoinduced Energy and Charge Transfer in P3HT:SWNT Composites. *J. Phys. Chem. Lett.* **2010**, *1*, 2406–2411.
17. Ren, S.; Bernardi, M.; Lunt, R. R.; Bulovic, V.; Grossman, J. C.; Gradecak, S. Toward Efficient Carbon Nanotube/P3HT Solar Cells: Active Layer Morphology, Electrical and Optical Properties. *Nano Lett.* **2011**, *11*, 5316–5321.
18. McNeill, C. R.; Abrusci, A.; Hwang, I.; Ruderer, M. A.; Muller-Buschbaum, P.; Greenham, N. C. Photophysics and Photocurrent Generation in Polythiophene/Polyfluorene Copolymer Blends. *Adv. Funct. Mater.* **2009**, *19*, 3103–3111.
19. Cheng, Y.; Prusoff, W. H. Relationship between Inhibition Constant (K_I) and Concentration of Inhibitor which Causes 50% Inhibition (I_{50}) of an Enzymatic-Reaction. *Biochem. Pharmacol.* **1973**, *22*, 3099–3108.
20. Flower, R. J. The Development of COX2 Inhibitors. *Nat. Rev. Drug Discovery* **2003**, *2*, 179–191.
21. Ju, S. Y.; Doll, J.; Sharma, I.; Papadimitrakopoulos, F. Selection of Carbon Nanotubes with Specific Chiralities Using Helical Assemblies of Flavin Mononucleotide. *Nat. Nanotechnol.* **2008**, *3*, 356–362.
22. Chen, F. M.; Zhang, W. J.; Jia, M. L.; Wei, L.; Fan, X. F.; Kuo, J. L.; Chen, Y.; Chan-Park, M. B.; Xia, A. D.; Li, L. J. Energy Transfer from Photo-Excited Fluorene Polymers to Single-Walled Carbon Nanotubes. *J. Phys. Chem. C* **2009**, *113*, 14946–14952.
23. Ohno, Y.; Iwasaki, S.; Murakami, Y.; Kishimoto, S.; Maruyama, S.; Mizutani, T. Excitonic Transition Energies in Single-Walled Carbon Nanotubes: Dependence on Environmental Dielectric Constant. *Phys. Status Solidi B* **2007**, *244*, 4002–4005.
24. Ando, T. Excitons in Carbon Nanotubes. *J. Phys. Soc. Jpn.* **1997**, *66*, 1066–1073.
25. Chuang, K. C.; Nish, A.; Hwang, J. Y.; Evans, G. W.; Nicholas, R. J. Experimental Study of Coulomb Corrections and Single-Particle Energies for Single-Walled Carbon Nanotubes Using Cross-Polarized Photoluminescence. *Phys. Rev. B* **2008**, *78*, 085411.
26. Hwang, J. Y.; Nish, A.; Doig, J.; Douven, S.; Chen, C.-W.; Chen, L. C.; Nicholas, R. J. Polymer Structure and Solvent Effects on the Selective Dispersion of Single-Walled Carbon Nanotubes. *J. Am. Chem. Soc.* **2008**, *130*, 3543–3553.
27. Schuettfort, T.; Snaith, H.; Nish, A.; Nicholas, R. Synthesis and Spectroscopic Characterization of Solution Processable Highly Ordered Polythiophene-Carbon Nanotube Nanohybrid Structures. *Nanotechnology* **2010**, *21*, 025201.
28. Weisman, R. B.; Bachilo, S. M. Dependence of Optical Transition Energies on Structure for Single-Walled Carbon Nanotubes in Aqueous Suspension: An Empirical Kataura Plot. *Nano Lett.* **2003**, *3*, 1235–1238.
29. Clark, J.; Silva, C.; Friend, R. H.; Spano, F. C. Role of Intermolecular Coupling in the Photophysics of Disordered Organic Semiconductors: Aggregate Emission in Regioregular Polythiophene. *Phys. Rev. Lett.* **2007**, *98*, 206406.
30. Bernardi, M.; Giulianini, M.; Grossman, J. C. Self-Assembly and its Impact on Interfacial Charge Transfer in Carbon Nanotube/P3HT Solar Cells. *ACS Nano* **2010**, *4*, 6599–6606.
31. Swaraj, S.; Wang, C.; Yan, H. P.; Watts, B.; Jan, L. N.; McNeill, C. R.; Ade, H. Nanomorphology of Bulk Heterojunction Photovoltaic Thin Films Probed with Resonant Soft X-Ray Scattering. *Nano Lett.* **2010**, *10*, 2863–2869.
32. Kim, Y.; Cook, S.; Choulis, S. A.; Nelson, J.; Durrant, J. R.; Bradley, D. D. C. Organic Photovoltaic Devices Based on Blends of Regioregular Poly(3-hexylthiophene) and Poly(9.9-dioctylfluorene-co-benzothiadiazole). *Chem. Mater.* **2004**, *16*, 4812–4818.
33. McNeill, C. R.; Greenham, N. C. Conjugated-Polymer Blends for Optoelectronics. *Adv. Mater.* **2009**, *21*, 3840–3850.
34. Salim, T.; Sun, S. Y.; Wong, L. H.; Xi, L. F.; Foo, Y. L.; Lam, Y. M. The Role of Poly(3-hexylthiophene) Nanofibers in an All-Polymer Blend with a Polyfluorene Copolymer for Solar Cell Applications. *J. Phys. Chem. C* **2010**, *114*, 9459–9468.
35. Ponder, J. W.; Richards, F. M. An Efficient Newton-Like Method for Molecular Mechanics Energy Minimization of Large Molecules. *J. Comput. Chem.* **1987**, *8*, 1016–1024.
36. Allinger, N. L.; Yuh, Y. H.; Lii, J. H. Molecular Mechanics—the MM3 Force-Field for Hydrocarbons 0.1. *J. Am. Chem. Soc.* **1989**, *111*, 8551–8566.
37. Beeman, D. Some Multistep Methods for Use in Molecular-Dynamics Calculations. *J. Comput. Phys.* **1976**, *20*, 130–139.
38. Bussi, G.; Donadio, D.; Parrinello, M. Canonical Sampling through Velocity Rescaling. *J. Chem. Phys.* **2007**, *126*, 014101.
39. Yang, M. J.; Koutsos, V.; Zaiser, M. Interactions between Polymers and Carbon Nanotubes: A Molecular Dynamics Study. *J. Phys. Chem. B* **2005**, *109*, 10009–10014.
40. Pettersen, E. F.; Goddard, T. D.; Huang, C. C.; Couch, G. S.; Greenblatt, D. M.; Meng, E. C.; Ferrin, T. E. UCSF Chimera—A Visualization System for Exploratory Research and Analysis. *J. Comput. Chem.* **2004**, *25*, 1605–1612.
41. Chang, M. H.; Hoffmann, M.; Anderson, H. L.; Herz, L. M. Dynamics of Excited-State Conformational Relaxation and Electronic Delocalization in Conjugated Porphyrin Oligomers. *J. Am. Chem. Soc.* **2008**, *130*, 10171–10178.